How to cite: *Angew. Chem. Int. Ed.* **2023**, *62*, e202307367
doi.org/10.1002/anie.202307367

Batteries **Hot Paper**

Hydrogen Transport and Evolution in Ni-MH Batteries by Neutron Imaging

Marin Nikolic, Alessia Cesarini, Emanuel Billeter, Fabian Weyand, Pavel Trtik, Markus Strobl, and Andreas Borgschulte**

Abstract: Efficiency losses due to side reactions are one of the main challenges in battery development. Despite providing valuable insights, the results of standard analysis on the individual components cannot be simply extrapolated to the full operating system. Therefore, non-destructive, and high resolution approaches that allow the investigation of the full system are desired. Herein, we combined neutron radiography and tomography with electrical monitoring of the state of charge of commercial Ni-mischmetal hydride batteries, to track the exchange and transport of hydrogen under operating conditions. This non-destructive approach allowed both the quantification of the hydrogen distribution in the electrodes in 4D, and the distinction between the electrochemically exchanged hydrogen and the hydrogen gas pressure generated by side reactions, as a function of the applied potential and current. One of the most counter-intuitive observation is that the generation of hydrogen gas during discharge depends on the charging state of the battery. The results presented provide critical new insights in the mechanisms governing the electrochemical processes during Nimischmetal hydride battery operation, and also pave the way for the extrapolation of this approach to the investigation of state-of-the-art Li-ions batteries.

Introduction

With the current focus towards renewable energy sources, the harvesting and storage of energy becomes pivotal. Great potential lies in the electrochemical energy storage in battery devices. However, the implementation on such a large scale shifts the focus of research and development from fundamental aspects to engineering challenges.[1] An unavoidable challenge of all electrochemical conversion devices is their miniaturization: the key processes take place at interfaces separated by defined and small distances. Upscaling is thus restricted to two dimensions. Batteries are based on established technologies utilizing smart concepts of packaging to minimize this effect. Despite this, side reactions of both electrochemical and non-electrochemical origin, as well as non-local parameters such as gas pressure, can have a significant impact on the overall performance. Therefore, in order to accurately assess and improve it, a comprehensive picture of the device is needed, both at the microscopic level of the individual components and at the overall macroscopic level.[2,3] Nickel-mischmetal hydride (Ni-MH) batteries are well established systems that consist of a Ni-M alloy and Nickel oxide hydroxide (NiOOH) separated by an alkaline electrolyte which provides ionic conductivity.[4–11] During charging, the positive electrode nickel hydroxide $Ni(OH)_2$ is oxidized with OH^- ions to NiOOH, water and an electron. The electron travels through an external circuit to the negative Ni-M electrode where reduction takes place to form the metal hydride MNi_5H_6 (Ni-MH) and the OH^- ions are regenerated. During discharge, the process is reversed. Effectively, a hydrogen is transported from one electrode to the other. The half-cell reactions are reversible (Table 1), thus the battery can be recharged after a partial or full discharge, making it suitable for applications where portable energy is needed.[7,8,10,11] A prerequisite for their applications is a large number of recharge cycles without loss of storage capacity.[7,12]

Nowadays, commercially available Ni-MH batteries have excellent rechargeability. This provides high reliability, stability, and durability without the use of precious or highly

[*] M. Nikolic, A. Cesarini, E. Billeter, F. Weyand, Dr. A. Borgschulte
Laboratory for Advanced Analytical Technologies, (Empa) Swiss Federal Laboratories for Material Science and Technology
Überlandstrasse 129, Dübendorf, 8600, Switzerland
E-mail: marin.nikolic@empa.ch
andreas.borgschulte@empa.ch

M. Nikolic
Department of Chemistry, University of Zürich
Winterthurerstrasse 190, Zürich, 8057, Switzerland
E-mail: marin.nikolic@empa.ch

A. Cesarini
Institute for Chemical and Bioengineering, Department of Chemistry and Applied Biosciences, ETH Zürich
Vladimir-Prelog-Weg 1–5/10, Zürich, 8093, Switzerland

F. Weyand
Institute of Environmental Engineering, ETH Zürich
Laura-Hezner-Weg 7, Zürich, 8093, Switzerland

Dr. P. Trtik, Dr. M. Strobl
Laboratory for Neutron Scattering and Imaging, Paul-Scherrer-Institute
Forschungsstrasse 111, Villigen, 5232, Switzerland

Table 1: Half-cell reactions and side reactions in a Ni-MH battery.[8,10,11] The Ni-mischmetal alloy is abbreviated here as MNi_5.

$\frac{1}{6}MNi_5H_6 + OH^- \rightleftharpoons \frac{1}{6}MNi_5 + e^- + H_2O$	$E^0 = -0.89$ V
$NiO(OH) + e^- + H_2O \rightleftharpoons Ni(OH)_2 + OH^-$	$E^0 = +0.44$ V
$\frac{1}{6}MNi_5H_6 + NiO(OH) \rightleftharpoons \frac{1}{6}MNi_5 + Ni(OH)_2$	$\Delta E^0 = +1.33$ V
$H_2 + \frac{1}{2}O_2 = \rightleftharpoons H_2O$	$E^0 = +1.23$ V

hazardous materials.[6] However, a severe disadvantage of Ni-MH batteries is their self-discharge rate.[8,10,11]

Furthermore, the improper operation of the battery, i.e., overdischarging, and overcharging, can result in hydrogen/oxygen gas evolution. In order to prevent the battery from exploding, a safety vent is installed to release the excess pressure.[8,10,11] To minimize these effects, the hydrogen evolution needs to be investigated on the full systems and not only on the materials level, since the hydrogen pressure depends on the absolute charging parameters, dead-volume and (catalytically active) surfaces present in the battery.[3] The phenomena that can be observed in Ni-MH batteries occur in most other battery systems as well, e.g. the decomposition of the electrolyte in Li-ion batteries.[13] In a recent work, Mattinen et al.[14] developed an operando cell house for on-line electrochemical mass spectrometry of a punctured battery. However, the largely increased dead-volume that is generated impedes the investigation of realistic pressure conditions. To observe gas formation in Li-ion batteries, Michalak et al.[15] performed neutron imaging studies to track and quantify gas formation in these batteries without the need of puncturing. Nevertheless, the study focused mainly on the gas formation during the evolution reactions and not on the chemical changes happening at the electrodes. In a similar study Senyshyn et al.,[16] investigated the evolution of the crystal structure of the anode and cathode material in a commercial Li-ion battery. However, the neutron diffraction and tomography experiments were performed at a fixed state of charge (SoC) which does not take into account the dynamic processes in between. Other proposed methods rely on optical measurements like Raman spectroscopy, which allow the operando chemical detection of hydrogen without modifying the dead-volume of the battery system.[17] Nevertheless, the overall battery setup had to be modified to include an optical window.

The large neutron scattering cross section for hydrogen compared to other elements[18,19] makes neutron radiography ideal as a non-destructive tool to probe gaseous as well as condensed hydrogen containing phases in the battery without further modifications.[20] In this work, we performed neutron imaging (combination of radiography and tomography) while monitoring the SoC of the battery under operating conditions to observe the electrochemical processes in the battery and bridge the knowledge gap. The measurements reveal the hydrogenation state of the electrodes as well as the hydrogen partial pressure in the battery in real time as a function of applied potential and current.

Results and Discussion

Galvanostatic charge-discharge measurements is the standard technique to monitor the SoC of a battery.[8,10,11,21] However, exact values of the discharge $Q_{discharge} = \int Idt < Q_{charge}$ deviate due to side reactions lowering the reversible charge stored in the electrodes. In this work, we show that the latter can be assessed by the hydrogen distribution derived from neutron tomography and compared to the global parameters exchanged charge ΔQ and voltage V.

Neutron tomography images of the battery such as pictured in Figure 1 were generated by taking images of the battery from different angles and later reconstructing the three-dimensional image and the neutron attenuation A_x:

$$A_x = \frac{\ln I_0/I}{d} \quad (1)$$

of each voxel using computer software[22] with d being the slice thickness and I_0 and I the neutron scattering intensity, without and with battery, respectively.

The 3D electrode/electrolyte and supporting structures were resolved with a resolution of 130 µm. Geometrical changes upon charging/discharging were found to be negligible ($\Delta l/l \simeq 0.2\,\%$). These changes can also be monitored by X-ray tomography; however the advantage of neutron imaging is in its specific element selectivity. The zebra-like structure of the electrodes as shown by sagittal and axial views of the battery (Figure 2) can be interpreted as the different hydrogen distributions. The neutrons are mainly scattered by hydrogen, the white zones correspond to higher neutron attenuation A_x (Eq. (1)) and indicate regions with high hydrogen content. Evidence of this interpretation is given by the contrast changes upon charging/discharging (Figure 1b and Figure 2), which provides a direct visual-

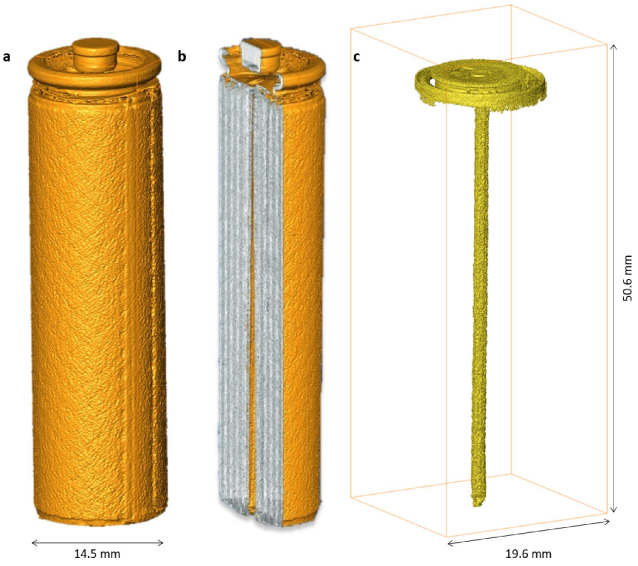

Figure 1. Neutron tomography of a commercial Ni-MH battery: **a**) complete view of the battery, **b**) saggital sliced view, **c**) visualization of the dead-volume.

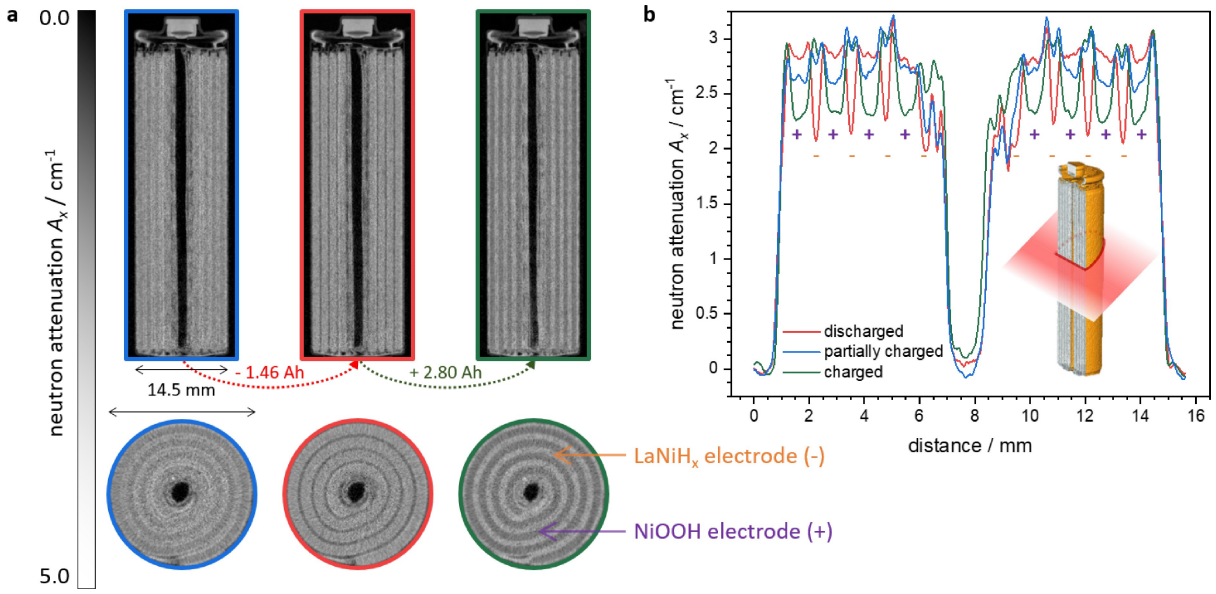

Figure 2. **a**) Saggital and axial view of a commercial Ni-MH battery at various SoC (blue: partially charged, red: discharged, green: charged) derived by neutron tomography. **b**) Neutron attenuation axially through the battery is shown in the graph for the battery at various SoC. The positive electrode is marked with a purple plus symbol, the negative electrode with an orange minus.

ization of the electrochemical hydrogen transfer in the Ni-MH battery (Table 1).

The contrast change combined with galvanostatic charge-discharge measurements, allows the simple assignment of negative (Ni-MH), and positive (NiOOH) electrode, respectively (Figure 2a). More details are given by axial line scans (Figure 2b) showing the hydrogen exchange between the electrodes, i.e., low, medium, and high neutron attenuation representing discharged, partially charged, and charged Ni-MH electrode, respectively. This behaviour is reversed for the oxide electrode. The center of the battery shows a less ordered behavior, probably due to the winding procedure during battery production which caused local deformations in the electrodes (see axial views in Figure 2).

In addition the neutron attenuation in the axial direction of the negative electrode at full charge is about 3 cm^{-1} (Figure 2b), which corresponds to $LaNi_5H_x$ with $x \approx 5$ (for calibration see Supporting Information, chapter 3). Although the calibration was not performed with exactly the same negative electrode material as in the commercial battery, and it did not take into account the contribution from the electrolyte wetting, this result shows that the neutron tomography method provides a precise quantification of the amount of hydrogen in the Ni-MH electrode itself.

As mentioned before, due to manufacturing the space of the battery cannot be fully filled with active material leaving a dead-volume (Figure 1c and Figure 2). These regions comprise also attenuation changes indicating a varying (partial) hydrogen pressure in the battery (Figure 2b). The limit of tomography is its long measurement time, which impedes time-resolved studies. Radiography perpendicular to the center axis of the battery delivers transmission images, which cannot fully resolve the cylindrical geometry of the electrodes. However, the top head space, as well as the outer electrode (Figure 3b) can be used to monitor the overall electrochemical changes in operando-mode since the areas are not affected by the interference caused by the neighbouring electrodes. The measured neutron absorbance A_n is derived from contrast measurements:

$$A_n(t) = \ln I_0/I(t) \tag{2}$$

zero neutron absorbance $A_n(0)$ is defined as with $I_0 = I(t=0)$ as the neutron scattering intensity at the start of the measurement. Assuming only hydrogen moving, the neutron absorption contrast can be converted into the amount of mobile hydrogen (concentration change c_H):

$$c_H = \frac{A_n}{\varepsilon \cdot d} = \frac{\ln I_0/I}{\varepsilon \cdot d} \tag{3}$$

with d the layer thickness and ε the neutron scattering cross section for hydrogen. ε depends on the energy of the neutrons used. The measurements were calibrated using hydrogen gas at room temperature and various pressures, and hydrogen exchange in $LaNi_5H_x$ (SI, chapter 3).

The charge exchanged in a battery is defined relative to the starting value ($\Delta Q(t=0) \equiv 0$). Each electron transferred corresponds to one H exchanged between the electrodes. The change of neutron absorbance is directly related to the hydrogen content (Eq. (2)). Furthermore, the neutron absorbance and the charge are directly proportional to each other (Figure 3 and Figure 4).

This relation is not found for the neutron absorbance caused by the hydrogen gas evolution in the battery. Hydrogen is an unavoidable gas in metal hydride batteries. Beside from the desired hydrogen exchange via ions,

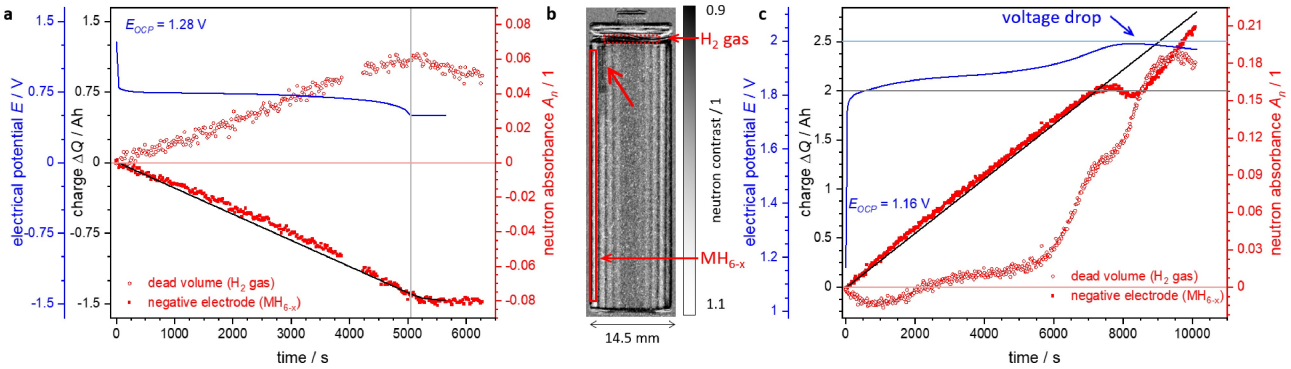

Figure 3. **a**, **c**) Neutron absorption of the outer negative electrode (indicated by the red rectangle with a solid line in the neutron radiography of the battery in **b**) and of the hydrogen gas in the top head space (indicated by the red rectangle with a dotted line in the neutron radiography of the battery in **b**) as a function of time, i.e. at different SoC. The battery was discharged at a current of $-C/2.3$ (**a**) and charged at $C/2.3$ (**c**). The corresponding discharge/charge voltage during operation is shown as blue line, while the charge removed from or added to the electrode is shown as a black line. **b**) Neutron radiography image of the battery at SoC $x = \Delta Q(t \approx 9000\ \text{s})$ from experiment **c**, where the greyscale corresponds to the neutron contrast, i.e. I_x/I_0. The red arrow indicates the area of increased neutron absorbance, most likely water accumulation.

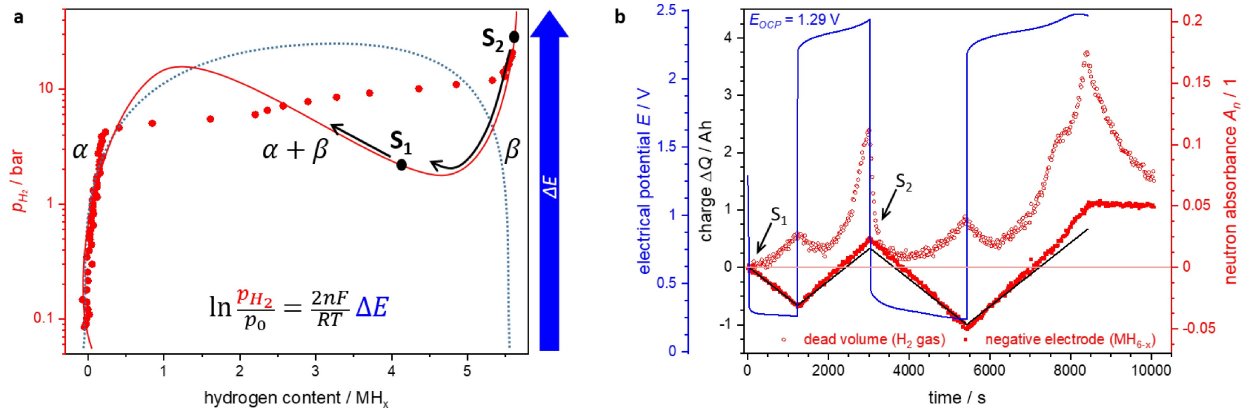

Figure 4. **a**) Hydrogen pressure-composition isotherm (pcT, red dots) of $LaNi_5H_x$ determined gravimetrically compared to the estimated initial SoC of the Ni-MH electrodes SoC $\mathbf{S_1}$ and $\mathbf{S_2}$. The red line illustrates the chemical potential of H in $LaNi_5$ following the pcT for the single phases. In the two phase regime, indicated by the blue line, the difference between chemical potential and the pcT indicates that supersaturation can occur.[24] **b**) Neutron absorption of the outer negative electrode and hydrogen gas in the upper headspace of the battery at different states of charge as a function of time while the battery was alternately discharged and charged at $\pm C/1.15$. The corresponding discharge/charge voltage during operation is shown in blue, while the charge removed from or added to the electrode is shown in black.

dihydrogen can be formed at the surface of the hydride. In equilibrium, the chemical potential of hydrogen gas μ_{H_2} is equal to that of hydrogen in the metal hydride linking equilibrium gas pressure to the stability of the hydride:[23]

$$\mu_{H_2} = 2\mu_H \tag{4}$$

$$\mu_{H_2} = \mu^0_{H_2} + RT \ln \frac{p_{H_2}}{p_0} \tag{5}$$

However, chemical and electrical potential E^0 are directly related:

$$E = E^0 + \frac{RT}{2nF} \ln \frac{p_{H_2}}{p_0} \tag{6}$$

The number of transferred electrons per hydrogen is $n = 1$, F is the Faraday constant. To reach as negative potentials as possible, hydrogen pressures close to ambient pressure are chosen.[7] Upon discharging, the metal hydride transforms into the low hydrogen concentration metal alloy, which implies that the equilibrium hydrogen pressure should decrease with discharging (Figure 4a). However, this decrease is not observed. Figure 3a shows an increase of the neutron absorbance of the hydrogen gas, i.e., the hydrogen partial pressure, which indicated that the amount of hydrogen in the dead-volume increases during discharge. According to the performed calibration (SI, chapter 3), a H_2 gas pressure of approximately 25 bar is derived. Furthermore, the hydrogen pressure starts to decrease again after the discharging is stopped (cutoff voltage at 0.5 V) indicative that the hydrogen gas further reacts at the electrodes. The latter observation shows a similar behaviour to the self-discharge process.[8,10,11]

However, this effect could be related to the SoC of the battery. In fact, the open circuit potential (OCP) of 1.28 V

which resembles a half-charged state. In order to understand its effect on the observed hydrogen pressure, one needs to take into consideration that the potential of the hydride electrode is directly linked to the equilibrium of the hydrogen metal alloy system (Eq. (6)). In this regard, a fully charged Ni-MH electrode corresponds to the single hydride phase, whereas the plateau corresponds to the two-phases regime where the hydride co-exist with a solid-solution phase (see pressure-composition isotherm of $LaNi_5H_x$ shown in Figure 4a). In such scenario, extracting hydrogen electrochemically at high currents perturbs the phase equilibrium resulting in a supersaturation,[24] as indicated by the point S_1 in Figure 4a, which represents the electrochemical state of the half charged Ni-MH electrode. When considering the discharge of a fully charged battery, the gas pressure initially decreases and it increases again when the plateau pressure is reached (Figure S3a). In this case, the electrochemical removal of hydrogen at high currents in a fully charged battery disturbs the phase equilibrium, leading first to undersaturation and then to supersaturation, as indicated by the points S_2 and S_1 (Figure 4a).

By reversing the process (recharge), hydrogen is intercalated back into the Ni-MH electrode. This is observed by the increase in neutron absorbance of the outer Ni-MH electrode, which directly correlates to the charge transferred (Figure 3c). This correlation does not hold anymore once the battery is fully charged (around 2000 mAh), as can be seen in Figure 3c. At this point, the battery begins to overcharge, which is also reflected in the voltage drop. At the same time, the neutron absorbance by hydrogen gas rises steeply. From the maximum value a hydrogen gas pressure of 70 bars is derived (for more details see Supporting Information chapters 3 and 4). This strong increase in neutron absorbance can be attributed to a high hydrogen partial pressure upon overcharging, which is in good agreement with literature.[8,10,11] Since the voltage increases to values well above 1.23 V, additional side reactions like the decomposition reaction of the electrolyte can occur (Table 1).

The high hydrogen pressure becomes reasonable when calculating the corresponding total amount of hydrogen formed in relation to the dead-volume. The latter, was calculated from the tomography analysis, which revealed a value of 0.2 cm^3 (Figure 1c). At 70 bar and a temperature close to 60 °C, this volume contains approximately 0.5 mmol of H_2. This corresponds to a charge of 0.03 Ah, which is negligible compared to the total charge ($\simeq$2.3 Ah).

Furthermore, dihydrogen evolution from H chemisorbed at the Ni-MH electrode competes with the intercalation of H into the metal hydride. For an substoichiometric Ni-MH electrode, intercalation and subsequent diffusion of H is faster than the formation of H_2 gas, since it does not require the slow recombination of atomic hydrogen into dihydrogen.[8,10,11] When reaching the single hydride phase, intercalation kinetics become slower, leading to higher coverage of hydrogen and thus easier formation of molecular hydrogen at the surface of the metal hydride. In addition, the concomitant oxygen evolution occurs when overcharging. Therefore, the capacity of the metal hydride is chosen to be slightly larger than that of the oxide electrode. This means that oxygen is formed once the full capacity is reached. To prevent the formation of explosive H_2/O_2 mixtures at high pressure, commercial Ni-MH batteries are equipped with a vent.[8,10,11] In addition to oxyhydrogen formation, another process to consider under overcharging conditions is the possible formation of water. For detailed discussion see chapter 4 of the SI.

In all the experiments carried out (Figure 3 and Figure 4), the safety vent did not open. It is important to note that the extreme conditions were used to demonstrate the effects. However, during battery discharge and charge, the gas pressure increase is proportional to the discharge and charge times both at extreme (Figure 3, Figure 4b) as well as normal operation conditions (Figure S3a).

In daily use, secondary batteries are charged and discharged multiple times. Such cycling processes were recreated and one of them is shown in Figure 4b. The cycling experiment is discussed in depth in chapter 5 of the Supporting Information and reflects all previously discussed hydrogen gas evolution and removal processes. In addition, the experiments highlight the importance of the charging history on the hydrogen partial pressure.

The approach herein presented allow battery systems to be analyzed operando under controlled conditions without affecting the battery, thus contributing to further optimization of the system. Furthermore, the time-resolved monitoring by neutron radiography of the dynamic processes involved during charging and discharging, combined with the tomography of the final states, provides a complete and detailed picture on the macroscopic as well as microscopic scale.

Conclusion

In conclusion, unravelling the complex phenomena occurring during a battery operation with information on current and voltage alone is challenging. The use of neutron imaging presented here for the operando monitoring of reaction processes, and the visualization of hydrogen transport in a Ni-MH battery proved to be an excellent, non-destructive and very easy to use imaging method with a great depth of details. We have shown how parameters such as structure and geometrical design of electrodes, electrolytes, separators, and containment, depend on the state of the battery and applied electrochemical conditions. By means of neutron tomography, the active material can easily be distinguished from the inactive one.

Moreover, the direct correlation between the neutron absorbance and the charge exchanged at the electrodes, allowed us to observe and describe the correlations between gas, charge, current, voltage and the SoC of the battery. The method reveals the undesirable side reactions during overcharging and discharging and the accumulation of side products. With neutron radiography, the corresponding hydrogen loss in the electrode was easily visualized, as well as the accompanying gas hydrogen evolution in the battery. Furthermore, while hydrogen evolution during electrolyte

decomposition is expected and indeed observed, the hydrogen gas evolution during discharge depends on the state of charge of the battery, giving insights for further improvement of its energy efficiency. The corresponding pressures are high and affect the charging voltage and exchanged hydrogen. The high hydrogen pressure is possible because of the small dead-volume of the battery confining the hydrogen generated by side reaction. This means that the battery chemistry is directly defined by the geometrical setup of the battery.

The results presented provide critical new insights in the mechanisms governing the electrochemical processes during Ni-MH batteries operation, and also pave the way for the extrapolation of this approach for the investigation of state-of-the-art Li-ions batteries. It is important to mention that for practical use, a user should avoid the extreme conditions we applied to showcase the effects.

Acknowledgements

The authors gratefully acknowledge financial support for the mega-move project from the ETHBoard (Board of the Swiss Federal Institutes of Technology). Additional funding via the UZH-UFSP program LightChEC and from the Swiss National Science Foundation [Grant no. 172662] was received. Open Access funding provided by ETH-Bereich Forschungsanstalten.

Conflict of Interest

The authors declare no conflicts of interest.

Data Availability Statement

The data that support the findings of this study are openly available in Zenodo at https://doi.org/10.5281/zenodo.8341235, reference number 8341235.

Keywords: nickel-mischmetal hydride battery · neutron Imaging · operando hydrogen mapping

[1] J. Frith, M. Lacey, U. Ulissi, *Nat. Commun.* **2023**, *14*, 420.
[2] D. Linden, T. Reddy, *Handbook of Batteries*, Electronics Book Series, McGraw-Hill **2002**.
[3] C. Grey, J. Tarascon, *Nat. Mater.* **2017**, *16*, 45.
[4] J. van Vucht, F. Kuijpers, H. C. Bruning, *Philips Res. Rep.* **1970**, *25*, 133.
[5] H. van Deutekom, P. Eindhoven, *The Netherlands* **1977**, patent file 7702259.
[6] G. Bronoel, J. Sarradin, M. Bonnemay, A. Percheron, J. Achard, L. Schlapbach, *Int. J. Hydrogen Energy* **1976**, *1*, 251.
[7] J. Willems, *Metal hydride electrodes stability of $LaNi_5$-related compounds*, Ph.D. thesis, Technische Hogeschool Eindhoven **1984**.
[8] P. Notten, *Rechargeable nickel-metalhydride batteries: a successful new concept*, pages 151–195, Springer Netherlands, Dordrecht **1995**.
[9] W. H. Zhu, Y. Zhu, Z. Davis, B. J. Tatarchuk, *Appl. Energy* **2013**, *106*, 307.
[10] P. Notten, J. Van Beek, *Chem. Ind.* **2000**, *54*, 102.
[11] P. Notten, M. Latroche, SECONDARY BATTERIES, NICKEL SYSTEMS, Nickel-Metal Hydride: Metal Hydrides, in J. Garche (Editor), *Encyclopedia of Electrochemical Power Sources*, pages 502–521, Elsevier, Amsterdam **2009**.
[12] D. Larcher, J. Tarascon, *Nat. Chem.* **2015**, *7*, 19–29.
[13] B. Rowden, N. Garcia-Araez, *Energy Reports* **2020**, *6*, 10.
[14] U. Mattinen, M. Klett, G. Lindbergh, R. Wreland Lindström, *J. Power Sources* **2020**, *477*, 228968.
[15] B. Michalak, H. Sommer, D. Mannes, A. Kaestner, T. Brezesinski, J. Janek, *Sci. Rep.* **2015**, *5*, 15627.
[16] A. Senyshyn, M. Mühlbauer, K. Nikolowski, T. Pirling, H. Ehrenberg, *J. Power Sources* **2012**, *203*, 126.
[17] *Vibrational spectroscopy of different classes and states of compounds*, chapter 4, pages 189–410, John Wiley and Sons, Ltd **1995**.
[18] E. Lehmann, P. Vontobel, N. Kardjilov, *Appl. Radiat. Isot.* **2004**, *61*, 503.
[19] S. F. Parker, D. Lennon, *Phys. Chem.* **2021**, *1*, 95.
[20] N. Kardjilov, I. Manke, A. Hilger, T. Arlt, R. Bradbury, H. Markötter, R. Woracek, M. Strobl, W. Treimer, J. Banhart, *Journal of Imaging* **2021**, *7*.
[21] X. Yang, A. L. Rogach, *Adv. Energy Mater.* **2019**, *9*, 1900747.
[22] P. Vontobel, E. H. Lehmann, R. Hassanein, G. Frei, *Physica B: Condensed Matter* **2006**, *385–386*, 475.
[23] R. Griessen, A. Driessen, *Phys. Rev. B* **1984**, *30*, 4372.
[24] R. Griessen, N. Strohfeldt, H. Giessen, *Nat. Mater.* **2016**, *15*, 311–317.

Manuscript received: May 25, 2023
Accepted manuscript online: September 15, 2023
Version of record online: October 6, 2023